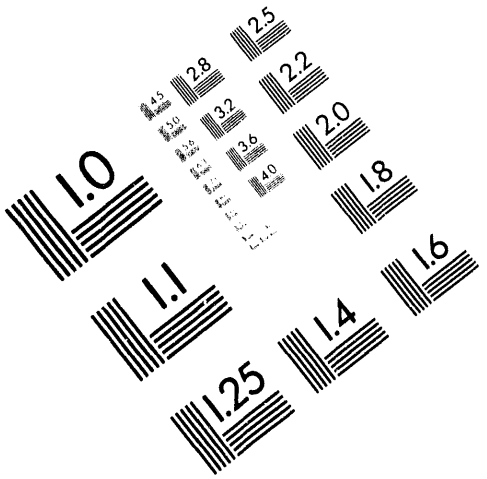

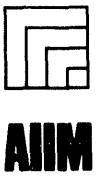

Association for Information and Image Management

1100 Wayne Avenue, Suite 1100
Silver Spring, Maryland 20910

301/587-8202

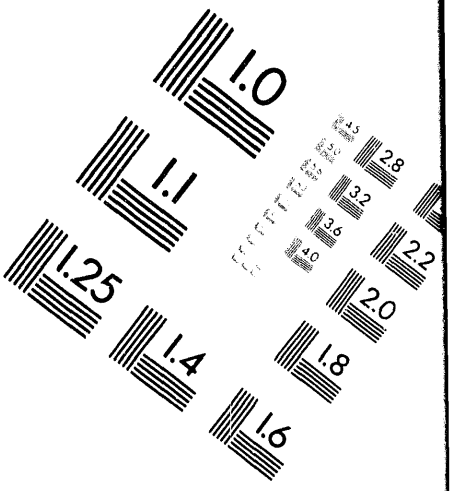

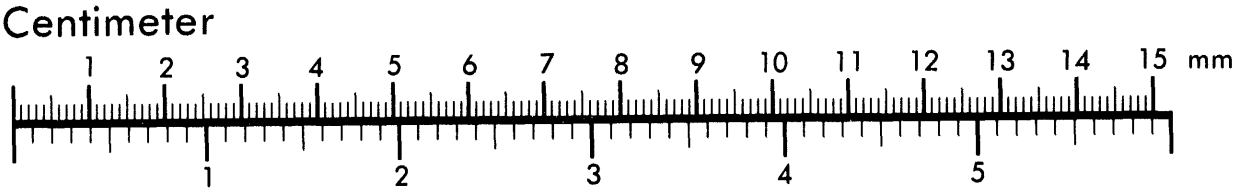

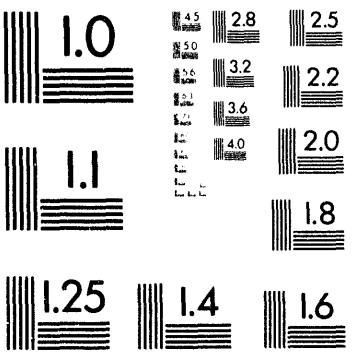

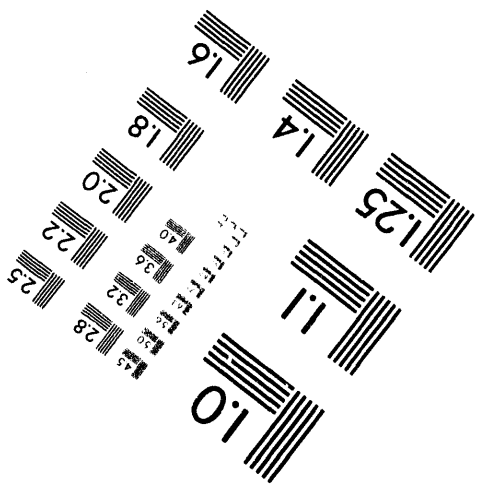

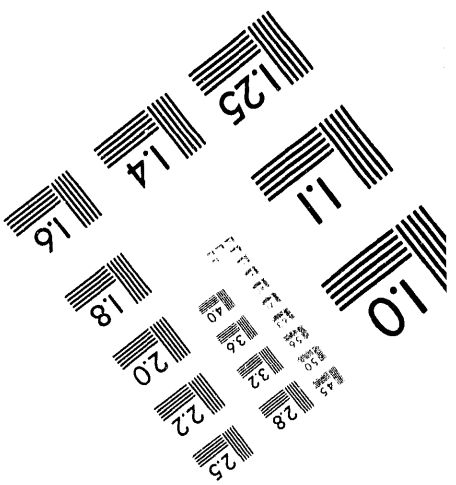

MANUFACTURED TO AIIM STANDARDS
BY APPLIED IMAGE, INC.

1 of 1

DEVELOPMENT OF A GAS-GENERATION MODEL FOR THE WASTE ISOLATION PILOT PLANT*

L. H. BRUSH,[1] J. W. GARNER,[2] AND L. J. STORZ[1]

1. Sandia National Laboratories, WIPP Gas Generation Program Department 6348, PO Box 5800, Albuquerque, NM 87185-1341
2. Applied Physics, Inc., 5353 Wyoming Blvd. NE, Suite 3, Albuquerque, NM 87109

ABSTRACT

Design-basis transuranic (TRU) waste to be emplaced in the Waste Isolation Pilot Plant (WIPP) in southeastern New Mexico may generate significant quantities of gas, which may affect the performance of the WIPP with respect to regulations for radioactive and/or chemically hazardous waste constituents. We are developing a model to predict gas generation in WIPP disposal rooms during and after filling and sealing. Currently, the model includes: (1) oxic and anoxic corrosion of steels and other Fe-base alloys, including passivation and depassivation; (2) microbial degradation of cellulosics with O_2, NO_3^-, $FeO(OH)$, SO_4^{2-}, or CO_2 as the electron acceptor; (3) α radiolysis of brine; (4) consumption of CO_2 and, perhaps, H_2S by $Ca(OH)_2$ (in cementitious materials) and CaO (a potential backfill additive). The code simulates these processes and interactions among them by converting reactants (steels, cellulosics, etc.) to gases and other products at experimentally observed or estimated rates and plotting temporal reaction paths in three-dimensional phase diagrams for solids in the Fe-H_2O-CO_2-H_2-H_2S system.

INTRODUCTION

Design-basis, defense-related TRU waste to be emplaced in the WIPP may generate significant quantities of various gases, perhaps a total of several hundred to a few thousand moles per drum of contact-handled (CH) TRU waste. Currently, there will be 6,804 equivalent drums of CH TRU waste per 3,644-m^3 WIPP disposal room. Furthermore, remote-handled (RH) TRU waste will be emplaced in the ribs (walls) of the 56 rooms and additional CH TRU waste will be emplaced in access drifts. Each room will contain about 2,300 m^3 of void volume immediately after emplacement of the waste and crushed-salt or crushed-salt-and-bentonite backfill. The reactions that generate gas may also produce or consume significant H_2O. By repressurizing the repository, gas may in turn affect the transport of brine and gas to or from the surrounding bedded-salt formation, the rate of room closure, and the geomechanical properties of the room contents and the surrounding formation after closure. Thus, gas generation may affect the performance of the WIPP with respect to regulations for radioactive constituents of the waste, and/or with respect to separate regulations for chemically hazardous constituents. Therefore, predictions of gas-generation rates and potentials are necessary for short- and long-term performance assessment of the WIPP.

*This work was supported by the United States Department of Energy under Contract DE-AC04-94AL85000.

Oxic and anoxic corrosion of steel waste containers (drums and boxes) and Fe and Fe-base alloys, Al and Al-base alloys, and, perhaps, other metals in the waste may produce H_2, and consume O_2, CO_2, H_2S, and H_2O. Aerobic and anaerobic microbial degradation of cellulosics and, perhaps, plastics and rubbers in waste boxes, drum liners, and the waste may produce CO_2, N_2, NH_3, H_2S, H_2, CH_4, and H_2O, and consume O_2, CO_2, H_2, and H_2O. Radiolysis of brine, cellulosics, plastics, and rubbers may produce H_2, O_2, and a variety of other gases, and consume H_2O. $Ca(OH)_2$ (in hydrated cementitious materials) and/or CaO (a potential backfill additive) may consume CO_2 and H_2S, and produce H_2O. Brush [1] described these processes in detail.

DESCRIPTION

We are developing a model to predict gas generation in WIPP disposal rooms during and after filling and sealing. The current version of this model includes: (1) oxic and anoxic corrosion of steels and other Fe-base alloys, including experimentally observed passivation by the adherent corrosion products $FeCO_3$ and FeS_2 and depassivation due to destabilization of these phases caused by changes in the composition of the gaseous phase; (2) microbial degradation of cellulosics with O_2, NO_3^-, FeO(OH), SO_4^{2-} or CO_2 as the electron acceptor; (3) brine radiolysis; (4) consumption of CO_2 by $Ca(OH)_2$ and/or CaO. Table I lists the reactions used to simulate these processes. For the calculations described below, we did not include microbial methanogenesis and brine radiolysis.

The code is written in Microsoft Fortran Version 5.1 for use on a personal computer. At the start of each time step, the code uses the fugacities of CO_2, H_2, and H_2S in the gaseous phase and thermodynamically calculated, three-dimensional phase diagrams for solid phases in the Fe-H_2O-CO_2-H_2-H_2S system to determine the solid corrosion product(s) stable during that time step. It then simulates anoxic corrosion and the other processes listed above by converting reactants (steels, cellulosics, H_2O, gases, etc.) to solid corrosion products, gases, and other products at rates observed in laboratory studies of gas generation for the WIPP Project [2, 3, 4, 5, 6], studies for other applications, or, if necessary, at estimated rates. The gases produced and consumed by these and other reactions in turn determine the fugacities of CO_2, H_2, and H_2S and the corrosion product(s) stable at the start of the next time step. In addition to these gases, the code calculates the quantities of other materials produced or consumed during each time step. These include other gases (O_2, N_2, and CH_4), H_2O, steels, other Fe-base alloys, corrosion products, microbial substrate, and microbial electron acceptors. It uses the ideal gas law to calculate individual gas fugacities and the total pressure. The code continues to convert reactants to gases and other products (or, in the case of gas-consuming reactions, it continues to convert gaseous reactants to nongaseous products) until a reactant is completely consumed or until that reactant is in equilibrium with the gaseous phase. The code predicts reaction paths by plotting points simultaneously depicting the common logarithms of the fugacities of CO_2, H_2, and H_2S (the gases that determine the stabilities of observed or possible corrosion products) in three-dimensional phase diagrams for the Fe-H_2O-CO_2-H_2-H_2S system after each time step. The graphics package used in conjunction with the code allows the user to rotate the axes of the phase diagrams and examine reaction paths from various perspectives. This has proven useful to verify that these paths lie on planar phase boundaries when two solid phases are present, or on linear intersections of these boundaries when three solids are present.

Table I.

Gas- and H_2O-Generation Reactions and Rates

Reaction	Rate (moles/drum·year)
Oxic corrosion:	
$2Fe + H_2O + 1.5O_2 = 2\gamma FeO(OH)$	H_2O: -20.0; O_2: -30.0
Anoxic corrosion:[1, 2]	
$Fe + 2H_2O = Fe(OH)_2 + H_2$	H_2O: -1.20; H_2: -0.600
$Fe + H_2O + CO_2 = FeCO_3 + H_2$	H_2O: -0.600; CO_2: -0.600; H_2: 0.600
$Fe + H_2S = FeS + H_2$	H_2S: -0.600; H_2: 0.600
$Fe + 2H_2S = FeS_2 + 2H_2$	H_2S: -0.600; H_2: 0.600
Microbial degradation:	
$C_6H_{10}O_5 + 6O_2 = 5H_2O + 6CO_2$	O_2: -0.500; H_2O: 0.417; CO_2: 0.500
$C_6H_{10}O_5 + 4.8H^+ + 4.8NO_3^-$ $= 7.4H_2O + 6CO_2 + 2.4N_2$	H_2O: 0.440; CO_2: 0.357; N_2: 0.143
$C_6H_{10}O_5 + 24FeO(OH) + 7H_2O$ $= 24Fe(OH)_2 + 6CO_2$	H_2O: -0.416; CO_2: 0.357
$C_6H_{10}O_5 + 24FeO(OH) + 18CO_2$ $= 24FeCO_3 + 17H_2O$	CO_2: -1.07; H_2O: 1.01
$C_6H_{10}O_5 + 24FeO(OH) + 24H_2S$ $= 24FeS + 41H_2O + 6CO_2$	H_2S: -1.43; H_2O: 2.44; CO_2: 0.357
$C_6H_{10}O_5 + 24FeO(OH) + 48H_2S$ $= 24FeS_2 + 41H_2O + 6CO_2 + 24H_2$	H_2S: -2.86; H_2O: 2.44; CO_2: 0.357 H_2: 1.43
$C_6H_{10}O_5 + 6H^+ + 3SO_4^{2-}$ $= 5H_2O + 6CO_2 + 3H_2S$	H_2O: 0.278; CO_2: 0.334; H_2S: 0.167
Consumption of CO_2:	
$Ca(OH)_2 + CO_2 = CaCO_3 + H_2O$	CO_2: -0.100; H_2O: 0.100

1. We have included possible formation of Fe_3O_4 in the model, but not in this simulation. Fe_3O_4 is stable with respect to $Fe(OH)_2$ at low fugacities of CO_2 and H_2S.
2. We have included reactions among corrosion products in the model, but have not shown them here. We currently assume that these reactions occur instantaneously at the end of a time step to adjust the fugacities of CO_2, H_2, and H_2S to values that simultaneously satisfy the equilibrium relationship(s) between or among these corrosion products.

In general, the current version of the gas-generation model assumes that equilibrium is attained after each incremental conversion of reactants in the system. In most cases, the code converts steels and other Fe-base alloys to the solid corrosion product(s) stable at the start of that time step. If two or more corrosion products are present at the end of a time step, the code adjusts the fugacities of CO_2, H_2, and H_2S to values that simultaneously satisfy the equilibrium relationship(s) for these corrosion products. It does this by converting one or more of these solid phases to another solid or solids present at that time in a manner analogous to a buffer. Only after one of these solids is completely consumed are the fugacities of CO_2, H_2, and H_2S free to deviate from values characteristic of equilibrium with that phase.

However, the model does include disequilibrium behavior observed in laboratory studies of gas generation. For example, at low fugacities of CO_2 and H_2S the code can, at the user's discretion, convert steels and other Fe-base alloys to $Fe(OH)_2$, the experimentally observed anoxic-corrosion product, despite the fact that $Fe(OH)_2$ is thermodynamically unstable with respect to Fe_3O_4 (magnetite) under these conditions. On the other hand, formation of Fe_3O_4 is also an option in the code to determine the effects of possible long-term conversion of $Fe(OH)_2$ to Fe_3O_4. Furthermore, the code simulates experimentally observed passivation of steels by "removing" these materials from the system once the experimentally observed passivation requirements are met (formation of enough $FeCO_3$ or FeS_2 on the surfaces of Fe-base materials to isolate them from additional corrosion). Furthermore, we will include other disequilibrium phenomena if necessitated by results from laboratory studies with actual or simulated TRU waste.

The gas-generation model is not a system-wide geochemical reaction-path model. Therefore, we will use models such as EQ3/6 to address issues other than gas generation, such as the effects of high CO_2 partial pressures on brine pH. We will then use experimental observations of, say, the effects of pH on corrosion rates to adjust the O_2-consumption and H_2-production rates from oxic and anoxic corrosion, respectively, in response to microbial CO_2 production. We will also use results from hydrologic and geomechanical models to determine the effects of two-phase (brine and gas) flow and room closure on the volume, brine content, and gas content of the repository.

PRELIMINARY RESULTS

Figure 1, Table II, and Figure 2 show predictions of gas generation in constant-volume WIPP disposal rooms. For these predictions, we used the gas-generation rates shown in Table I and estimates of the initial quantities of nonradioactive waste constituents shown in the first column of Table II. These rates and inventory estimates are preliminary and may change as more results are obtained from laboratory studies of gas generation and from waste-characterization studies. In this simulation, microbial activity consumed all of the available cellulosics, but anoxic corrosion consumed only a minor portion of the metallic Fe initially present (Table I) due to inhibition and, eventually, passivation. Other outcomes are possible. Microorganisms may eventually consume the plastics and rubbers to be emplaced in WIPP disposal rooms, thus producing significantly more microbial gas than shown in Table I and significantly higher partial and total pressures than shown in Figure 1. Methanogenesis could significantly affect the quantities and types of gases. Proposed backfill additives such as CaO may decrease the quantity of CO_2, but may depassivate steels and other Fe-base alloys, thus restarting anoxic corrosion.

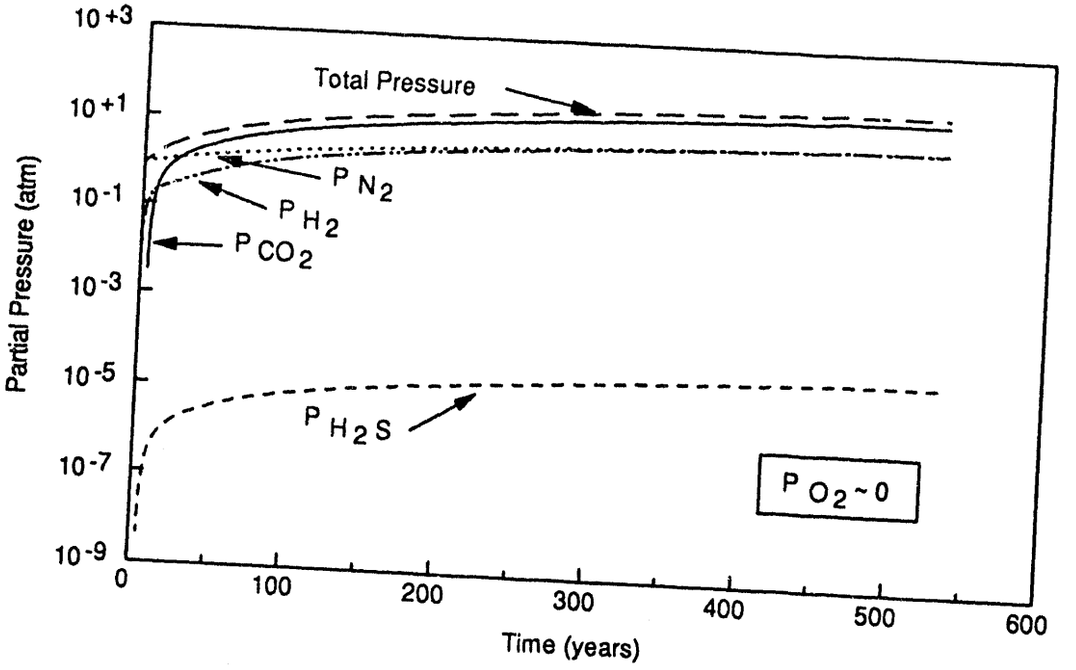

Figure 1. Predictions of Partial and Total Pressures as a Function of Time.

Table II.

Quantities of Nonradioactive Constituents as a Function of Time

Constituent	Quantity (moles/drum)					
	0 yr	0.1 yr	6.1 yr	8.2 yr	48.0 yr	535.1 yr
Fe	1,250	1,250	1,250	1,250	1,240	1,160
FeO(OH)	0.000	3.53	0.000	0.000	0.000	0.000
$Fe(OH)_2$	0.000	0.000	0.000	0.000	0.000	0.000
$FeCO_3$	0.000	0.0798	4.40	4.68	2.30	1.99
FeS	0.000	0.0167	1.02	1.37	8.00	8.92
FeS_2	0.000	0.000	0.000	0.000	0.000	0.000
$C_6H_{10}O_5$	61.7	61.7	60.9	60.6	56.0	0.000
NO_3^-	182	182	181	180	169	29.4
SO_4^{2-}	119	119	118	118	111	30.0
$Ca(OH)_2$	4.80	4.79	4.19	3.98	0.000	0.000
$CaCO_3$	0.000	0.0100	0.610	0.820	4.80	4.80
CO_2	0.00400	0.0400	0.0400	1.10	27.0	364
H_2	0.000	0.0488	1.85	2.48	6.73	87.6
H_2O	1,260[2]	1,260	1,260	1,260	1,300	1,650
H_2S	0.000	0.000	0.000	0.000	0.000	0.000
N_2	10.3	10.3	11.2	11.5	17.1	86.7
O_2	2.72	0.000	0.000	0.000	0.000	0.000

1. For the initial quantity of H_2O, we used the sum of H_2O expected in the waste at the time of emplacement and that expected to seep in from the surrounding formation prior to repressurization.

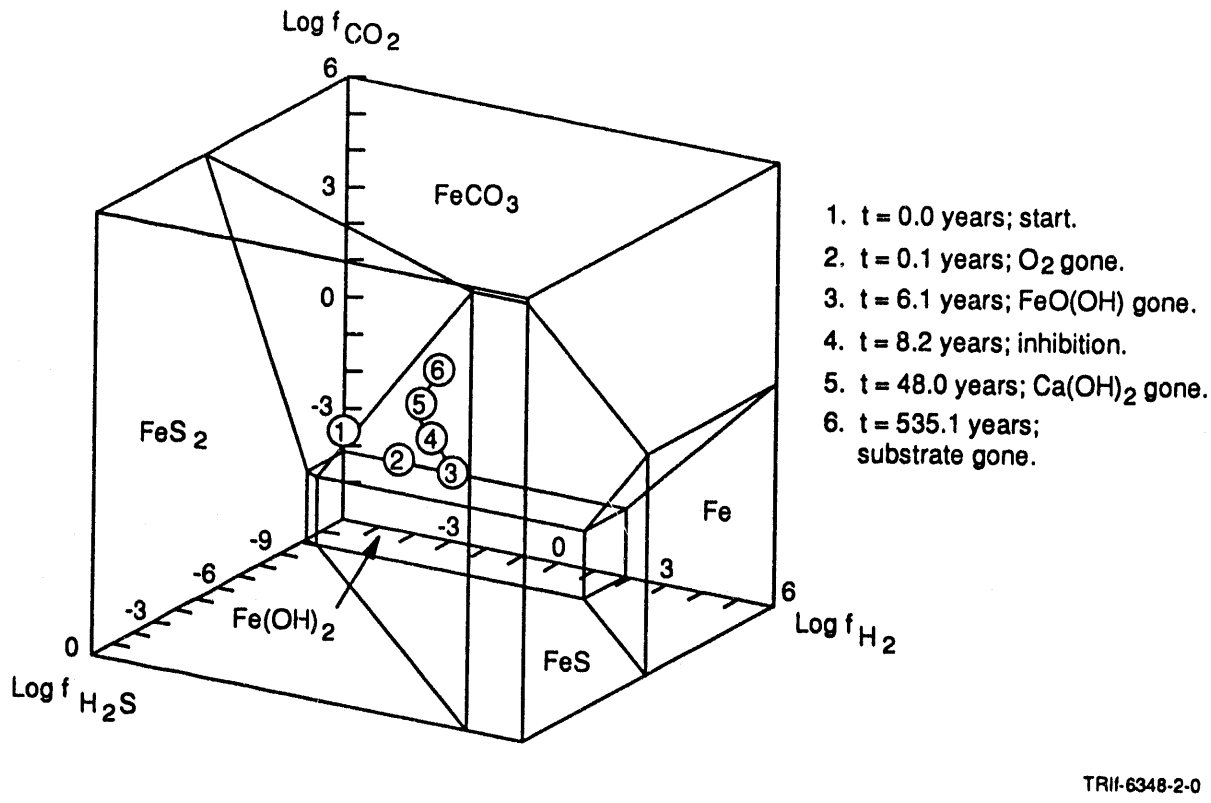

Figure 2. Predicted Reaction Path in the Phase Diagram for Solid Phases in the Fe-H_2O-CO_2-H_2-H_2S System. We assumed that metastable $Fe(OH)_2$ persists throughout the entire 535.1-year-long run. Point 1 is in $FeCO_3$ space; points 2 through 6 are on the $FeCO_3$-FeS plane.

REFERENCES

1. L. H. Brush, **Test Plan for Laboratory and Modeling Studies of Repository and Radionuclide Chemistry for the Waste Isolation Pilot Plant**, SAND90-0266 (Sandia National Laboratories, Albuquerque, NM, 1990).
2. M. A. Molecke, **Gas Generation from Transuranic Waste Degradation: Data Summary and Interpretation**, SAND79-1245 (Sandia National Laboratories, Albuquerque, NM, 1979).
3. L. H. Brush, M. A. Molecke, R. E. Westerman, A. J. Francis, J. B. Gillow, R. H. Vreeland, and D. T. Reed, in **Scientific Basis for Nuclear Waste Management XVI**, ed. by C. G. Interrante and R. T. Pabalan (Mater. Res. Soc. Proc., 294, Pittsburgh, PA, 1993), pp. 335 to 340.
4. D. T. Reed, S. Okajima, L. H. Brush, and M. A. Molecke, "Radiolytically-Induced Gas Production in Plutonium-Spiked WIPP Brine," in **Scientific Basis for Nuclear Waste Management XVI**, op. cit., pp. 431-438.
5. M. R. Telander and R. E. Westerman, **Hydrogen Generation by Metal Corrosion in Simulated Waste Isolation Pilot Plant Environments: Progress Report for the Period November 1989 through December 1992**, SAND92-0266 (Sandia National Laboratories, Albuquerque, NM, 1993).
6. A. J. Francis and J. B. Gillow, **Effects of Microbial Processes on Gas Generation under Expected WIPP Repository Conditions: Annual Report through 1992**, SAND93-7036 (Sandia National Laboratories, Albuquerque, NM, 1993).

DATE

FILMED

7/15/94

END